"Smart" Base Isolation Strategies Employing Magnetorheological Dampers

H. Yoshioka[1]; J. C. Ramallo[2]; and B. F. Spencer Jr.[3]

Abstract: One of the most successful means of protecting structures against severe seismic events is base isolation. However, optimal design of base isolation systems depends on the magnitude of the design level earthquake that is considered. The features of an isolation system designed for an El Centro-type earthquake typically will not be optimal for a Northridge-type earthquake and vice versa. To be effective during a wide range of seismic events, an isolation system must be adaptable. To demonstrate the efficacy of recently proposed ''smart'' base isolation paradigms, this paper presents the results of an experimental study of a particular adaptable, or smart, base isolation system that employs magnetorheological (MR) dampers. The experimental structure, constructed and tested at the Structural Dynamics and Control/Earthquake Engineering Laboratory at the Univ. of Notre Dame, is a base-isolated two-degree-of-freedom building model subjected to simulated ground motion. A sponge-type MR damper is installed between the base and the ground to provide controllable damping for the system. The effectiveness of the proposed smart base isolation system is demonstrated for both far-field and near-field earthquake excitations.

DOI: 10.1061/(ASCE)0733-9399(2002)128:5(540)

CE Database keywords: Damping; Base isolation; Earthquake excitation.

Introduction

Seismic base isolation is one of the most successful techniques to mitigate the risk to life and property from strong earthquakes (Skinner et al. 1993; Naeim and Kelly 1999). In base isolation systems, nonlinear devices such as lead-rubber bearings, friction-pendulum bearings, or high damping rubber bearings are often used. The benefit of these types of bearings is that the restoring force and adequate damping capacity can be obtained in one device. However, because the dynamic characteristics of these devices are strongly nonlinear, the vibration reduction is not optimal for a wide range of input ground motion intensities. The features of an isolation system designed for an El Centro-type earthquake typically will not be optimal for a Kobe-type earthquake and vice versa. Indeed, the effectiveness of many passive base isolation systems has been questioned for near-source, high-velocity, long period pulse earthquakes (Hall et al. 1995; Heaton et al. 1995).

Because the performance of highly sensitive equipment in hospitals, communication centers, and computer facilities can be easily disrupted by moderate acceleration levels and even permanently damaged by higher excitations (Inaudi and Kelly 1993), efforts have turned toward the use of isolation for protection of a building's contents. For example, base isolation systems have been employed in a semiconductor facility in Japan to reduce microvibration from a nearby high-speed train rail (Furuhashi et al. 1998). Recent revisions to the Uniform Building Code (ICBO 1997) mandate the accommodation of larger base displacements and the consideration of a stronger maximum credible earthquake (MCE), indirectly suggesting the need for supplemental damping devices. However, the addition of damping to minimize base displacements may increase both internal deformation and absolute accelerations of the superstructure, thus defeating many of the gains for which base isolation is intended (Naeim and Kelly 1999). In general, protection of the contents of a structure is achieved through minimization of structural accelerations.

Seeking to develop isolation systems that can be effective for a wide range of ground excitations, hybrid control strategies, consisting of a passive isolation system combined with actively controlled actuators, have been investigated by a number of researchers (e.g., Kelly et al. 1987; Inaudi and Kelly 1990; Nagarajaiah et al. 1993; Yang et al. 1996; Nishimura and Kojima 1998). The advantages of hybrid base isolation systems are high performance in reducing vibration, the ability to adapt to different loading conditions, control of multiple vibration modes of the structure, and so on. Several small-scale experiments have been performed to verify the effectiveness of this class of systems in reducing structural responses. Inaudi and Kelly (1990) investigated active base isolation of a four-story building model employing an electrohydraulic actuator. Nagarajaiah et al. (1993) applied this idea to a bridge model with steel and Teflon bearings and a hydraulic actuator. Yang et al. (1996) examined sliding mode controllers for a four-story base-isolated building model employing a hydraulic actuator. However, such active control devices typically require a large external power supply during extreme seismic events. Moreover, active systems have the additional risk of instability.

[1]Visiting Scholar, Dept. of Civil Engineering and Geophysical Sciences, Univ. of Notre Dame, Notre Dame, IN 46556; on leave from Takenaka Corporation, Research and Development Institute, Chiba, Japan.

[2]Research Associate, Laboratorio de Estructuras, Univ. Nacional de Tucumán, Avenue Roca 1800, (4000) San Miguel de Tucumán, Tucumán, Argentina.

[3]Leo Linbeck Professor of Civil Engineering, Univ. of Notre Dame, Notre Dame, IN 46556.

Note. Associate Editor: James L. Beck. Discussion open until October 1, 2002. Separate discussions must be submitted for individual papers. To extend the closing date by one month, a written request must be filed with the ASCE Managing Editor. The manuscript for this paper was submitted for review and possible publication on December 13, 2000; approved on September 13, 2001. This paper is part of the ***Journal of Engineering Mechanics***, Vol. 128, No. 5, May 1, 2002. ©ASCE, ISSN 0733-9399/2002/5-540–551/$8.00+$.50 per page.

Another class of hybrid base isolation systems employs semiactive control devices, often termed ''smart'' dampers. Semiactive systems have the capability of adapting to changes in external loading conditions, similar to the active protective system, but without requiring access to large power supplies. Feng et al. (1993) reported an analytical and experimental study of a controllable-friction bearing in an isolation system. Controllable fluid dampers employing electrorheological (ER) fluids (Gavin et al. 1996; Gavin 2001) or magnetorheological (MR) fluids (Spencer et al. 1997) have been suggested to control damping force. Some researchers have applied these devices to develop smart base isolation systems (Yang et al. 1995, 1996; Makris 1997; Johnson et al. 1999; Symans and Kelly 1999; Yoshida et al. 1999; Ramallo et al. 2000a,b; Yang and Agrawal 2001). Nagarajaiah et al. (2000) experimentally showed the effectiveness of semiactive base isolation for a single span bridge model using MR dampers. Several shaking table tests were also conducted with smart dampers in base-isolated building models (Madden et al. 2000; Sahasrabudhe et al. 2000). However, systematic experimental comparison with an optimal passive damping system has not been investigated, nor has the performance of these systems been considered for various ground motion intensities.

This paper experimentally investigates smart base isolation strategies employing MR dampers for protection of building structures. The experimental structure, constructed and tested at the Structural Dynamics and Control/Earthquake Engineering Laboratory at the Univ. of Notre Dame, is a base-isolated two-degree-of-freedom building model. The sponge-type MR damper used in this study has a particularly simple design. A clipped-optimal control strategy is used to reduce structural acceleration, while maintaining base drifts within an acceptable limit. To demonstrate the efficacy of this system, responses due to simulated ground motions with several intensities are presented. The effectiveness of the proposed smart base isolation system is demonstrated through comparison with optimal passive dampers for both far-field and near-field earthquake excitations.

Experimental Setup

In this section, the experimental setup of the smart base isolation model is presented. Experiments were conducted on the shaking table at the Structural Dynamics and Control/Earthquake Engineering Laboratory (SDC/EEL) at the Univ. of Notre Dame. The uniaxial earthquake simulator consists of a hydraulic actuator/servo-valve assembly that drives a 122×122 cm^2 aluminum slip table mounted on high-precision, low-friction linear bearings. The capabilities of the simulator are ±5.1 cm maximum displacement, ±89 cm/s maximum velocity, and ±4 g maximum acceleration with a 454.5 kg test load. The operational frequency range of the simulator is nominally 0–50 Hz.

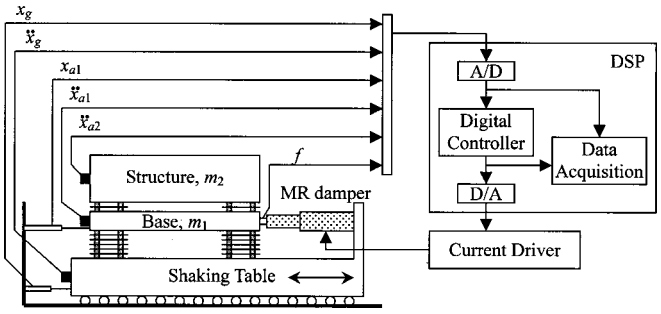

Fig. 2. Schematic of experimental setup

The test structure shown in Figs. 1 and 2 is a two-mass model supported by laminated rubber bearings. This model represents a five-story prototype structure with an isolation period of 2 s. The first mass ($m_1=10.5$ kg) corresponding to the isolation base of the structure consists of a $32\times32\times2.5$ cm^3 aluminum plate. The second mass ($m_2=57.5$ kg) represents a single-degree-of-freedom (one-mode) model of the superstructure and consists of one $32\times32\times2.5$ cm^3 steel plate and two $30\times32\times2.5$ cm^3 steel plates. Twenty-layer laminated rubber bearings are employed as isolators at each of the four corners of the base. Each layer consists of three neoprene rubber disks with a height of 0.3 cm and a diameter of 1.1 cm attached to a $10.2\times7.7\times0.1$ cm^3 steel plate. The experimentally verified shear modulus of the neoprene rubber is 0.11 N/mm^2. Because the vertical stiffness of the isolation bearings is relatively low, a linear guide is installed below the base to restrict vertical and torsional motion. The top mass, m_2, was then mounted on two-layer laminated rubber bearings and attached to the lower mass, m_1. This approach keeps the center of gravity of the structure low, minimizing overturning moments in the model. Therefore, only the horizontal motion of the base and the structure is considered in this experiment.

Capacitive accelerometers are installed in the horizontal direction on the base mass m_1 and the upper mass m_2. A piezoelectric accelerometer is also attached in the horizontal direction on the shaking table. The base displacement is determined by taking the difference between the output of the laser displacement sensor measuring the absolute displacement of the base and the LVDT measuring the shaking table displacement.

An MR damper is attached between the base and the table to control the response of the structure. As shown in Fig. 3, this MR damper employs absorbent foam saturated with the MR fluid. The force generated by a MR damper is controlled via a current driver. The characteristics of the damper are ±3.5 cm maximum stroke,

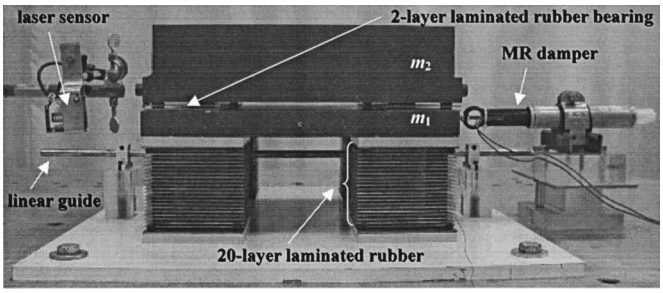

Fig. 1. Experimental setup of smart base isolation system

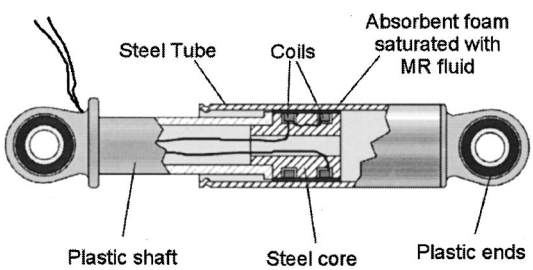

Fig. 3. Schematic of magnetorheological sponge damper

Table 1. Similitude Relations for Experimental Model

	Identified experimental model	Assumed prototype structure	Ratio
Time	1	3	$\alpha = 1/3$
Displacement	1	20.4	$\gamma = 1/20.4$
Velocity	1	6.8	γ/α
Acceleration	1	2.27	γ/α^2
First mode frequency (Hz)	1.4197	0.47323	$1/\alpha$
Second mode frequency (Hz)	11.65	3.8833	$1/\alpha$
First mode damping (%)	1.51	1.51	1
Second mode damping (%)	2.99	2.99	1
Fundamental frequency of fixed superstructure (Hz)	5.19	1.73	$1/\alpha$
m_1: Mass of the base (kg)	10.5	105,000[a]	$\beta = 0.001$[a]
m_2: Mass of the structure (kg)	57.5	575,000[a]	$\beta = 0.001$[a]
m: $m_1 + m_2$ (kg)	68.0	680,000[a]	$\beta = 0.001$[a]
Maximum force of the magnetorheological damper (kgf)	4.5	102,000	$\beta\gamma/\alpha^2$
Maximum damper stroke (cm)	3	61.2	γ

[a]Parameter β can be chosen arbitrarily.

50 N maximum force with a current of 0.5 A. The applied force generated by the MR damper is measured by a piezoelectric load cell.

Digital control is achieved by a dSPACE control system, which uses a Texas Instruments TMS320C40 DSP chip and I/O boards with 16-bit A/D and D/A converters. Discrete-time controllers are implemented in *SIMULINK*-based coding software. The sampling rate is set to 1 kHz.

The similitude relations between the model and the prototype structure for time scale, mass, and length are

$$\alpha = t'/t$$

$$\beta = m'/m \tag{1}$$

$$\gamma = x'/x$$

where t, m, and x = time, mass, and length, respectively, in the prototype structure, and the primed quantities are those for the model structure (Szucs 1980). Table 1 shows the similitude relations for the experimental model.

Control Design Model

A two-degree-of-freedom model of the structure is employed for the purpose of control design. The behavior of both the structure and the isolation bearings is assumed to be linear. The state space representation of the equation of motion for the linear base isolation system as shown in Fig. 4 is given by

$$\dot{\mathbf{X}} = \mathbf{A}\mathbf{X} + \mathbf{B}f + \mathbf{E}\ddot{x}_g \tag{2}$$

$$\mathbf{X} = [x_1 \quad x_2 \quad \dot{x}_1 \quad \dot{x}_2]^T$$

$$\mathbf{A} = \begin{pmatrix} \mathbf{0} & \mathbf{I} \\ -\begin{bmatrix} \omega_1^2 + \omega_2^2\mu & -\omega_2^2\mu \\ -\omega_2^2 & \omega_2^2 \end{bmatrix} & -\begin{bmatrix} 2\zeta_1\omega_1 + 2\zeta_2\omega_2\mu & -2\zeta_2\omega_2\mu \\ -2\zeta_2\omega_2 & 2\zeta_2\omega_2 \end{bmatrix} \end{pmatrix} \tag{3}$$

$$\mathbf{B} = [0 \quad 0 \quad 1/m_1 \quad 0]^T, \quad \mathbf{E} = [0 \quad 0 \quad -1 \quad -1]^T$$

$$\mu = \frac{m_2}{m_1}, \quad \omega_1^2 = \frac{k_1}{m_1}, \quad \omega_2^2 = \frac{k_2}{m_2}, \quad 2\zeta_1\omega_1 = \frac{c_1}{m_1}, \quad 2\zeta_2\omega_2 = \frac{c_2}{m_2} \tag{4}$$

where x_1 and x_2 = displacement of the base and structure relative to the ground, respectively; f and x_g = control force applied by damper and the absolute ground displacement, respectively; and m_1, m_2, k_1, k_2, c_1, and c_2 = mass, stiffness, and damping coefficients for the base and the structure.

The optimization for these parameters was performed using the multi-input–multi-output identification method (Ramallo et al., unpublished work) based on the Nelder-Mead simplex algorithm (Coleman et al. 1999), which is available in *MATLAB*.

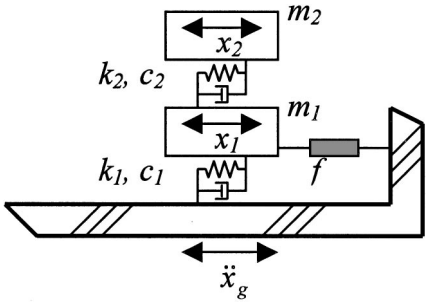

Fig. 4. 2DOF linear base isolation model

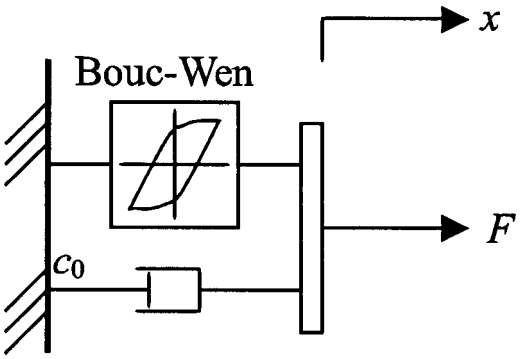

Fig. 5. Magnetorheological damper model with Bouc-Wen hysteresis (Spencer et al. 1997)

Several mathematical models have been proposed for controllable fluid dampers. Spencer et al. (1997) developed an effective model using the Bouc-Wen hysteresis model for MR fluid dampers. Because of the simple configuration of the MR damper used in this experiment, the damper dynamics can be represented with a combination of the Bouc-Wen model and a viscous damping element as shown in Fig. 5. This model is a special case of the model proposed by Spencer et al. (1997) and subsequently employed by Yi et al. (unpublished). The force generated by the MR damper is modeled as

$$F = c_0\dot{x} + \alpha z$$
$$\dot{z} = -\gamma|\dot{x}|z|z|^{n-1} - \beta\dot{x}|z|^n + A\dot{x} \quad \text{or} \tag{5}$$
$$\dot{z} = \{A - |z|^n[\gamma\ \text{sgn}(\dot{x}z) + \beta]\}\dot{x}$$

The parameters of the MR damper model were identified by Ramallo et al. (unpublished) to be $A=1$, $n=1$, $\gamma=\beta=58.662\ \text{cm}^{-2}$, and $c_0=0.3327$ N s/cm. A small time lag exists between the command and the damper force due to the inductance in the coil in the damper's electromagnet and the time constant of the fluid. This lag is modeled with a first-order filter between the control voltage v and the parameter α (N/cm) representing the damper yield level given by

$$\dot{\alpha}(t) = -[\alpha(t) - p_1 v(t) - p_2]\eta \tag{6}$$

where $\eta = 2\pi \times 11.0$ (rad/s); $p_1 = 3111.7$ (N/cm/V); and $p_2 = 161.47$ (N/cm).

The effectiveness of this numerical model for representing the dynamic behavior of the MR damper is verified in Ramallo et al. (unpublished).

Optimal Passive Base Isolation System

As the baseline to evaluate the effectiveness of the smart base isolation system, a passive base isolation system employing the MR damper subjected to a constant current is experimentally examined. Note that because the MR damper operating at a constant current behaves like a yielding device, this passive isolation system can be viewed as approximation the response of a base isolation system with lead rubber bearings. The NS component of the El Centro earthquake with two intensities is considered, as well as the NS component of the JMA Kobe earthquake record.

Fig. 6(a) shows the maximum acceleration response due to the strong El Centro earthquake. The maximum ground acceleration is 0.2 g, which corresponds to 0.45 g for the prototype structure. A constant current of 0.25 A is optimal for reducing the maximum acceleration of the structure. This design is considered the optimal passive against which the smart base isolation strategies are compared.

Although the passive isolation system performs well for the large-amplitude ground motion, as shown in Fig. 6(b), this damping level is not optimal for reducing structural acceleration due to more moderate earthquakes. Here, the structure is subjected to the El Centro earthquake scaled to have a maximum ground acceleration of 0.07 g, which corresponds to 0.2 g for the prototype structure.

Fig. 7 shows the maximum base displacement due to both the strong and moderate earthquakes. To reduce base displacement, the constant current applied to the MR damper should be large. Generally speaking, to concurrently reduce base displacement and structural acceleration is difficult past a certain level of reduction.

In the next section, the design of a smart base isolation system is considered that can effectively achieve reduction in base displacements and structural accelerations during a broad range of earthquake intensities.

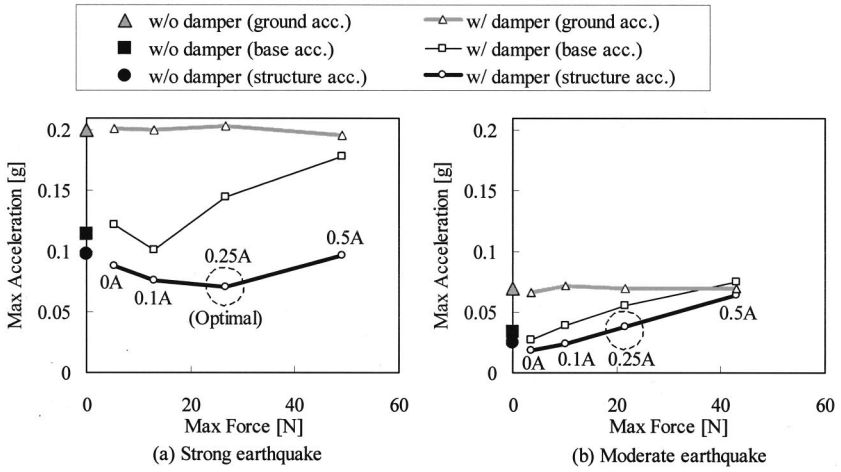

Fig. 6. Experimental maximum absolute acceleration responses due to scaled El Centro NS record with magnetorheological damper operated in passive mode

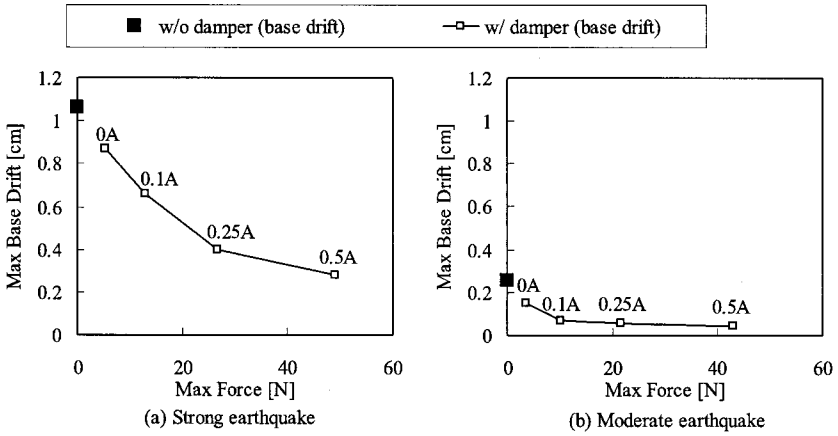

Fig. 7. Experimental maximum base drift due to scaled El Centro NS record with magnetorheological damper operated in passive mode

Smart Damping Strategy

Because smart damping devices such as MR dampers have highly nonlinear characteristics, a number of different control strategies have been proposed. Dyke and Spencer (1997) compared several control algorithms appropriate for a MR damper and concluded that a clipped-optimal controller with a bang-bang force-tracking scheme is most suitable for this class of damper. This clipped-optimal controller employs a desired optimal control force that is determined using linear optimal control design strategies (e.g., H_∞, H_2/LQG, μ-synthesis, etc.), and then subsequently clips the force to accommodate the intrinsic dissipative nature of smart damping devices.

For the experiment described herein, a clipped-optimal controller employing the H_2/LQG strategy (Dyke et al. 1996) is used to reduce structural responses. Spencer et al. (2000) and Ramallo et al. (2000a,b) showed through simulation that this approach is effective for smart base isolation systems. The basic concept of this methodology is shown in Fig. 8 and described in the following paragraphs.

For purposes of control design, the input excitation is modeled as a filtered white noise. The excitation shaping filter is written in state space form as

$$\dot{\xi} = \mathbf{A}_W \xi + \mathbf{B}_W w$$
$$\ddot{x}_g = \mathbf{C}_W \xi \tag{7}$$

where w = scalar white noise excitation. Combining Eq. (7) with Eq. (2), the augmented system becomes

$$\begin{bmatrix} \dot{\mathbf{X}} \\ \dot{\xi} \end{bmatrix} = \begin{bmatrix} \mathbf{A} & \mathbf{E}\mathbf{C}_W \\ \mathbf{0} & \mathbf{A}_W \end{bmatrix} \cdot \begin{bmatrix} \mathbf{X} \\ \xi \end{bmatrix} + \begin{bmatrix} \mathbf{B} \\ \mathbf{0} \end{bmatrix} f + \begin{bmatrix} \mathbf{0} \\ \mathbf{B}_W \end{bmatrix} w \tag{8}$$

Defining $\mathbf{X}_s = [\mathbf{X}^T \; \xi^T]^T$, Eq. (8) can be written as

$$\mathbf{X}_s = \mathbf{A}_s \mathbf{X}_s + \mathbf{B}_s f + \mathbf{E}_s w \tag{9}$$

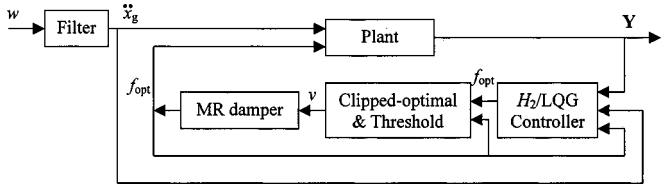

Fig. 8. H_2/LQG strategy with clipped-optimal switching

The measured outputs for the controller are the absolute accelerations of the base, the structure, and the ground

$$\mathbf{Y} = \begin{bmatrix} \ddot{x}_1 + \ddot{x}_g \\ \ddot{x}_2 + \ddot{x}_g \\ \ddot{x}_g \end{bmatrix} = \begin{bmatrix} \mathbf{C}_1 & \mathbf{0} \\ \mathbf{C}_2 & \mathbf{0} \\ \mathbf{0} & \mathbf{C}_W \end{bmatrix} \cdot \begin{bmatrix} \mathbf{X} \\ \xi \end{bmatrix} + \begin{bmatrix} 1/m_1 \\ 0 \\ 0 \end{bmatrix} f + \mathbf{v} \tag{10}$$

or

$$\mathbf{Y} = \mathbf{C}_Y \mathbf{X}_s + \mathbf{D}_Y f + \mathbf{v} \tag{11}$$

where $\mathbf{v}$ = measurement noise.

The responses to be regulated are the displacements, velocities, and accelerations of the base and structure. Then, the regulated outputs are represented as

$$\mathbf{Z} = \mathbf{C}_Z \mathbf{X}_s + \mathbf{D}_Z f \tag{12}$$

The performance index to be minimized in selecting the desired optimal force f_{opt} is given by

$$J = \lim_{\tau \to \infty} \frac{1}{\tau} E\left[\int_0^\tau \{\mathbf{Z}^T \mathbf{Q} \mathbf{Z} + r f^2\} dt \right] \tag{13}$$

where Q and r = weightings for regulated outputs and damper force. The desired optimal force using the H_2/LQG strategy is given by

$$f_{opt} = -\mathbf{K}\hat{\mathbf{X}}_s \tag{14}$$

where $\hat{\mathbf{X}}_s$ = state vector estimated by the Kalman filter.

To track the optimal force f_{opt}, Dyke et al. (1996) proposed a clipped-optimal switching, defined by

$$v = V_{max} H\{(f_{opt} - f_{meas}) f_{meas}\} \tag{15}$$

where v = voltage to the current driver associated with saturation of the magnetic field in the MR damper, and $H(\bullet)$ is the Heaviside step function. This control algorithm has the benefit that a model of the damper is not required in the control design. Because the sensor outputs in the experiment include some dc offset and noise, the desired force also includes an offset as well as noise. The influence of these errors is significant in the case of small vibration. Thus, the controller may send an incorrect signal to the damper, especially for ambient vibration. In this experiment, an alternative clipped-optimal control with a threshold is proposed in which the control voltage remains zero below minimum force, f_{min}, i.e.,

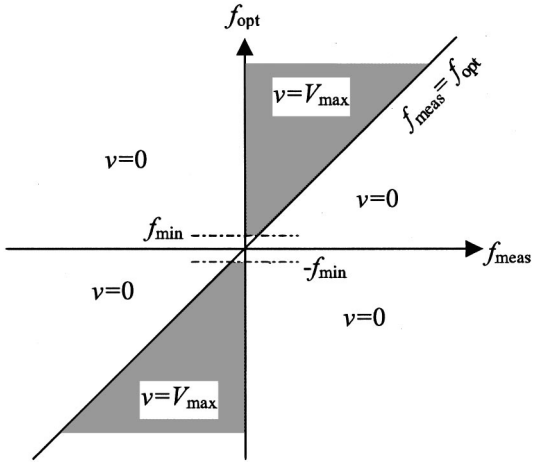

Fig. 9. Clipped-optimal controller with threshold strategy

$$v=\begin{cases} V_{max}H\{(f_{opt}-f_{meas})f_{meas}\}, & |f_{opt}|>f_{min} \\ 0 & \text{otherwise} \end{cases} \tag{16}$$

A schematic of the proposed clipping scheme is shown in Fig. 9. Herein, the minimum force is set to 4.3 N.

Historical earthquake records are used for the input motion. As the shaking table uses displacement feedback, the acceleration records have to be integrated twice and scaled before being sent to the shaking table. To avoid divergence due to the dc component of the signal in the integration, a high-pass filter with a cutoff frequency of 0.3 Hz is applied to the acceleration records. The power spectral density (PSD) of the experimental acceleration is compared with earthquake records in Fig. 10. The PSD of the experimental acceleration is less at low frequencies. In contrast, the PSD of the experimental acceleration is larger at the higher frequencies. However, satisfactory reproduction of the acceleration is achieved at the frequencies of the first two modes of the structure. For control design purposes, the input shaping filter $W(s)$, whose transfer function is also shown in Fig. 10, is assumed to model the ground motion, i.e.,

$$W(s)=\frac{75.2717}{s+75.2717}\,\frac{s}{s+33.2899} \tag{17}$$

Because the MR damper can only produce dissipative forces, the optimal control force designed by the H_2/LQG method and then clipped is not guaranteed to be the optimal control for the smart damping system. Therefore, an optimal switching plane is sought by examining several weightings for the H_2/LQG controller. Numerical results for the simulated El Centro NS earthquake with a maximum acceleration of about 0.2 g are shown in Fig. 11. Several controllers with different weighting are investigated. Most of the controllers using the proposed clipped-optimal control strategy, especially in the case of velocity weighting of the base, can reduce acceleration of the base and structure more effectively than the passive system. However, the controller commanding the largest forces does not reduce acceleration response effectively. From these simulation results, the optimal controller that reduces both the maximum and RMS structural acceleration is obtained by weighting the velocity of the base as shown in Fig. 11 and designated with the circle. This controller can also reduce base acceleration better than passive mode. This optimal control design is used for all of the experimental results for the smart isolation system reported in this paper.

For implementation on the digital controller, the controller is transformed to a discrete time controller using the bilinear transformation (Quast et al. 1995) to obtain

$$\mathbf{X}_{k+1}^{s}=\mathbf{A}^{s}\mathbf{X}_{k}^{s}+\mathbf{B}^{s}\mathbf{Y}_{k}$$
$$f_{k}^{opt}=\mathbf{C}^{s}\mathbf{X}_{k}^{s} \tag{18}$$

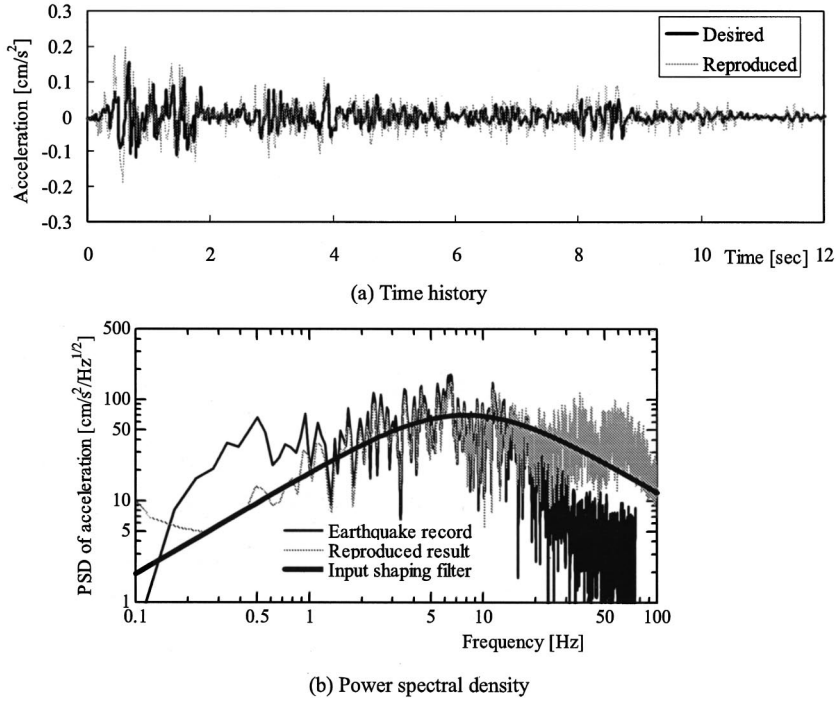

Fig. 10. Reproduced acceleration and input shaping filter (El Centro NS component, time scale factor: 1/3)

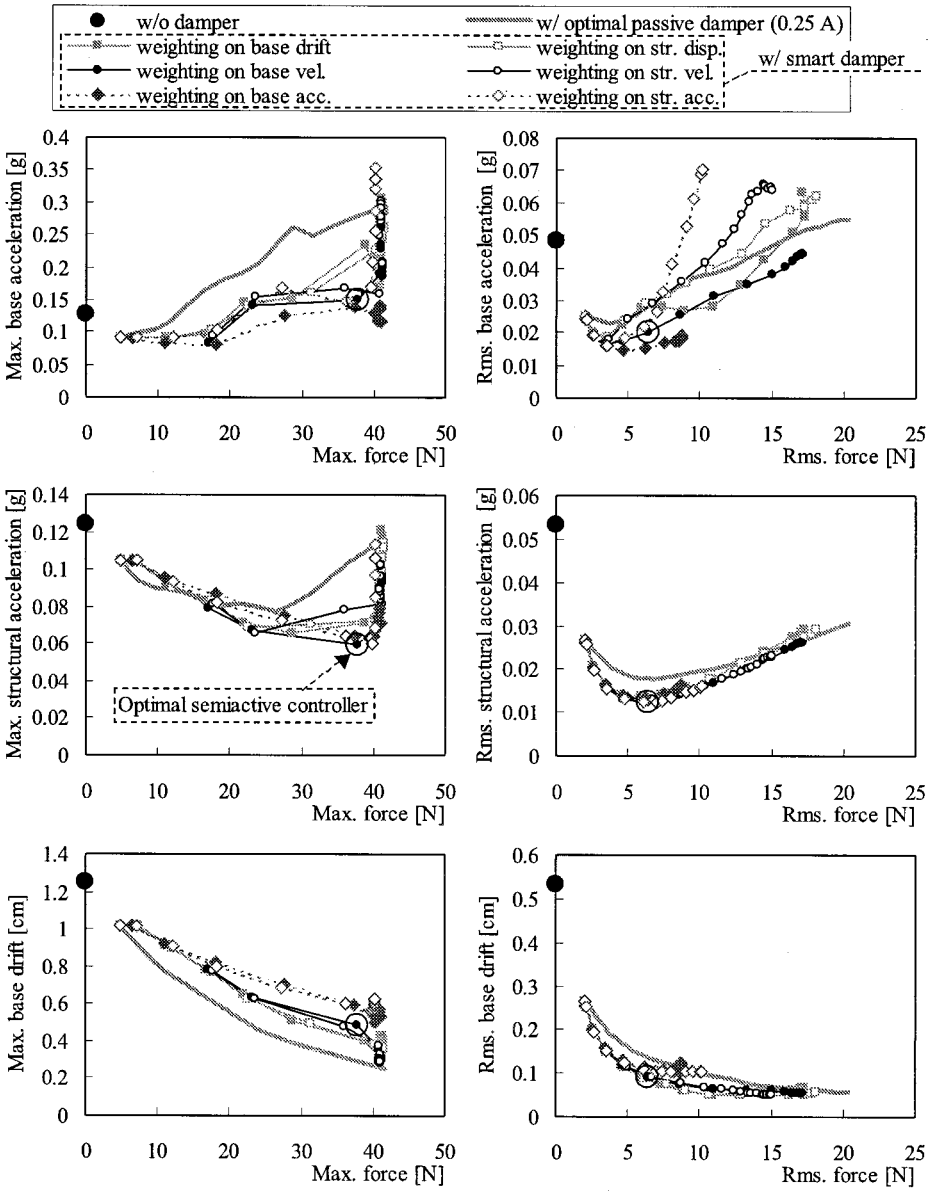

Fig. 11. Numerical response for simulated El Centro NS earthquake record with maximum acceleration of 0.2 g

Experimental Results

The proposed smart base isolation system employing MR dampers was experimentally investigated and compared with the optimal passive base isolation system with the MR damper operated in constant current mode. To demonstrate the effectiveness of this system for different levels and types of seismic events, three earthquake records are considered:

1. Strong El Centro NS: maximum ground motion is scaled to 0.2 g (0.44 g for prototype);
2. Moderate El Centro NS: maximum ground motion is scaled to 0.07 g (0.16 g for prototype); and
3. Strong JMA Kobe NS: maximum ground motion is scaled to 0.46 g (1.04 g for prototype).

As described previously, the passive damper employed in this experiment is experimentally optimized for the *strong* El Centro NS earthquake record (see circles marked in Fig. 6). The smart damping strategies investigated herein were designed using the procedure described in the previous section to minimize the structural acceleration due to the *strong* El Centro NS earthquake record (see Fig. 11).

Fig. 12 shows experimental results for the smart isolation system subjected to the strong El Centro NS earthquake record. As seen here, the measured force provided by the MR damper tracks the desired control force commanded by the clipped-optimal strategy quite well. Compared to the case without the damper, acceleration response and base drift are reduced substantially. The maximum structural acceleration is reduced from 96.2 cm/s^2 (without damper) to 52.5 cm/s^2 (with smart damper). Compared to the input ground acceleration (peak acceleration of 198.5 cm/s^2), the peak acceleration for the structure employing the smart damper showed an attenuation of 73.6%.

Figs. 13 and 14 compare experimental results for optimal passive and smart damping strategies. Tables 2 and 3 summarize the

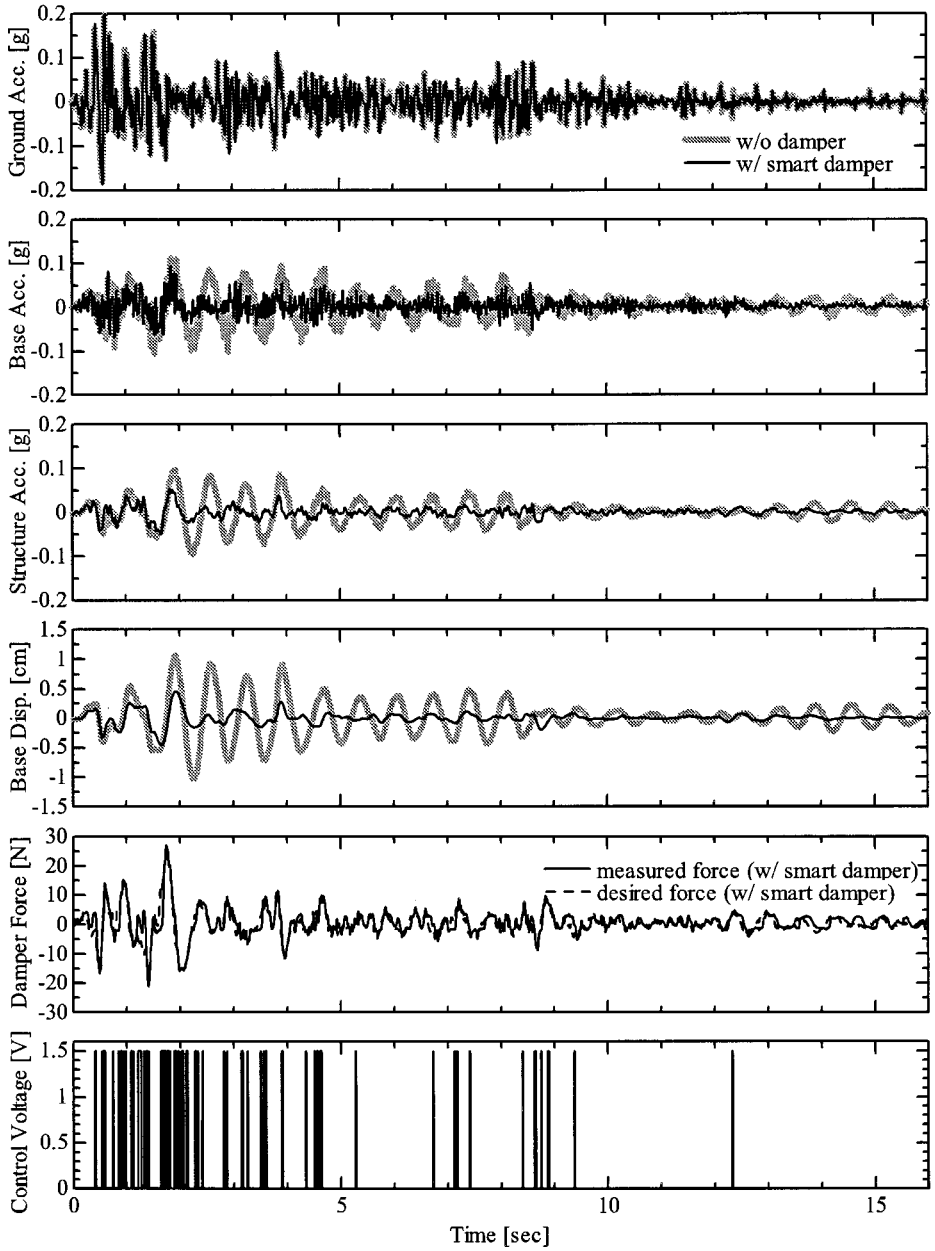

Fig. 12. Experimental result due to strong El Centro NS earthquake record

maximum and RMS responses. The passive damper optimized for the strong El Centro NS earthquake record can reduce the acceleration response due to the target earthquake. However, in the case of the moderate El Centro NS earthquake record, the base and structural accelerations for the optimal passive system are worse than the corresponding responses with no damper installed. On the contrary, the smart isolation system can reduce responses due to both the strong and moderate El Centro NS earthquake records. Compared to the optimal passive system, acceleration reductions for the smart isolation systems range from 25–35% better in the case of the strong earthquake, and 45–60% better in the case of the moderate earthquake. For the JMA Kobe NS earthquake record with a maximum acceleration of 455.6 cm/s^2, which corresponds to 1,034 cm/s^2 for the prototype structure, the smart isolation system can achieve from 10 to 25% better performance than the optimal passive damper.

Note that the optimal passive hysteretic damper generates almost the same maximum force for all three earthquake records. On the other hand, the smart isolation system adapts to the situation, generating smaller forces for the case of a moderate earthquake and larger forces for strong earthquakes. Although this property is similar to the passive viscous dampers, Spencer et al. (2000) showed that the viscous dampers are not as effective as the smart base isolation systems. Note that during a moderate earthquake, although the base drift of the smart isolation system is larger than for the optimal passive system, it is still smaller than the base drifts during a severe earthquake. Indeed, one would like to have larger drifts during a seismic event, so long as the seismic gap of the isolation system is not exceeded.

Fig. 15 shows the PSD of the acceleration response due to both the strong and the moderate El Centro NS earthquake records. The first mode is dominant in the acceleration response

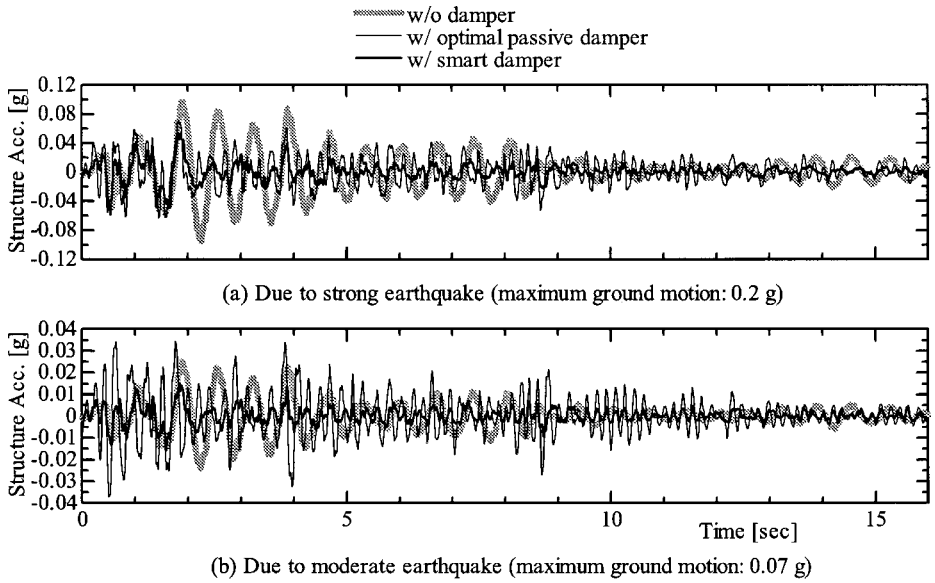

Fig. 13. Experimental acceleration response of structure due to scaled El Centro NS earthquake records

without the damper. In both cases, the passive and smart controllers can reduce this first mode response well. However, the response is amplified, as compared to the case without the damper, in the frequency range from 2 to 8 Hz for the case with the optimal passive damper. This tendency is particularly notable for a moderate earthquake. This frequency range encompasses the natural frequency of the fixed based superstructure, 5.2 Hz (see Table 1). Therefore, because the damping force generated by the passive damper is relatively large in the case of a moderate earthquake, the superstructure is behaving, to a great extent, as a fixed base structure. In the case of a smart damper, responses at higher frequencies are much smaller.

Fig. 16 shows how the input ground acceleration is attenuated in the structure. The percent attenuation of the peak structural accelerations over the peak input ground acceleration is shown versus the peak acceleration of the El Centro earthquake scaled to various levels. As seen here, the passive hysteretic dampers optimized for a strong earthquake cannot effectively reduce the struc

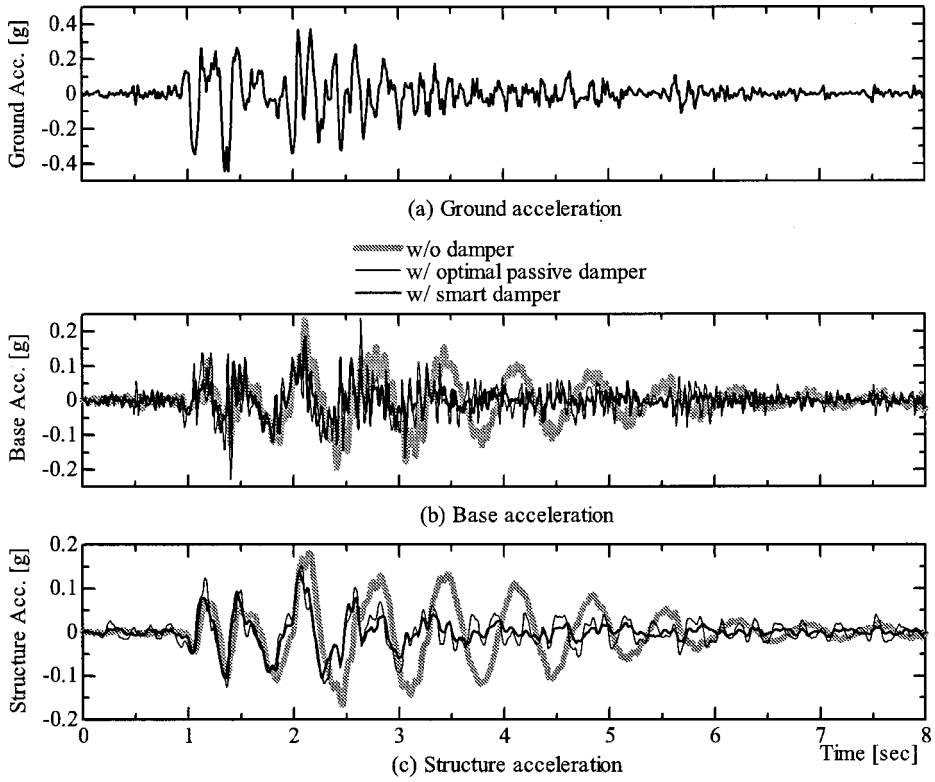

Fig. 14. Experimental acceleration response of structure due to JMA Kobe NS earthquake record

Table 2. Maximum Experimental Structural Response due to Simulated Earthquakes

El Centro NS	El Centro NS	El Centro NS	JMA Kobe NS
		Ground acceleration (cm/s^2)	
	68.76	198.5	455.6
		Baseacceleration(cm/s^2)	
Without damper	33.41	111.6	236.4
Optimal passive	54.94	142.2	237.4
Magnetorheological damper	30.56(44.4)	89.0(37.4)	179.5(24.4)
		Structuralacceleration(cm/s^2)	
Without damper	24.93	96.24	179.9
Optimal passive	37.18	69.47	150.4
Magnetorheological damper	15.73(57.7)	52.49(24.4)	134.5(10.6)
		Basedrift(cm)	
Without damper	0.2558	1.0639	1.953
Optimal passive	0.0556	0.3988	1.135
Magnetorheological damper	0.0979(−76.1)	0.4567(−14.5)	1.117(1.6)
		Damperforce(N)	
Optimal passive	21.56	26.74	28.88
Magnetorheological damper	7.30	27.30	40.07

Note: % reduction over optimal passive defined by (Optimal Passive−MR Damper)/Optimal Passive×100.

tural acceleration response due to moderate earthquakes. On the other hand, the smart damping system is effective for the entire range of earthquakes, indicating that the smart damping control strategy is quite insensitive to the magnitude of the ground motion.

Conclusions

The performance of a smart isolation system for the base-isolated two-degree-of-freedom structural model employing MR fluid dampers has been investigated. The efficacy of this smart base isolation system in reducing the structural responses for a wide range of loading conditions has been demonstrated in a series of experiments conducted at the Structural Dynamics and Control/Earthquake Engineering Laboratory at the Univ. of Notre Dame. An analytical model of the MR damper employing the Bouc-Wen hysteresis has been presented. A modified clipped-optimal control strategy has been proposed and shown to be effective. By applying a threshold to the control voltage for the MR damper, the controller becomes robust for the ambient vibration. The dynamic behavior of this system is also shown to be predictable. Results for the smart isolation system were compared to those where the MR damper was operated in a passive mode (i.e., with a constant

Table 3. Root Mean Square Experimental Structural Response due to Simulated Earthquakes

El Centro NS	El Centro NS	El Centro NS	JMA Kobe NS
		Ground acceleration (cm/s^2)	
	10.13	32.43	89.72
		Base acceleration (cm/s^2)	
Without damper	7.66	28.02	55.04
Optimal passive	9.08	24.99	45.01
Magnetorheological damper	5.69 (37.3)	16.47 (34.1)	31.29 (30.5)
		Structural acceleration (cm/s^2)	
Without damper	6.59	26.92	57.68
Optimal passive	9.81	19.96	36.60
Magnetorheological damper	3.35 (65.9)	10.91 (45.3)	29.24 (20.1)
		Base drift (cm)	
Without damper	0.0722	0.3047	0.6587
Optimal passive	0.0093	0.0713	0.2843
Magnetorheological damper	0.0200 (−115.1)	0.0965 (−35.3)	0.2670 (6.1)
		Damper force (N)	
Optimal passive	5.82	11.04	14.92
Magnetorheological damper	1.36	4.39	10.84

Note: % reduction over optimal passive defined by (Optimal Passive−MR Damper)/Optimal Passive×100.

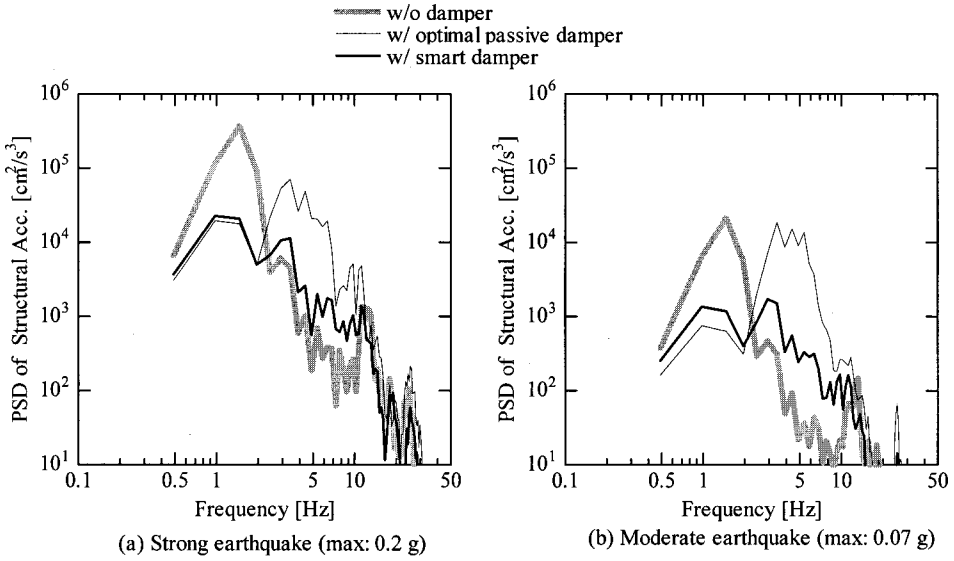

Fig. 15. Power spectral density of structural acceleration due to El Centro NS (2048 point data averaged eight times with 1 kHz sampling)

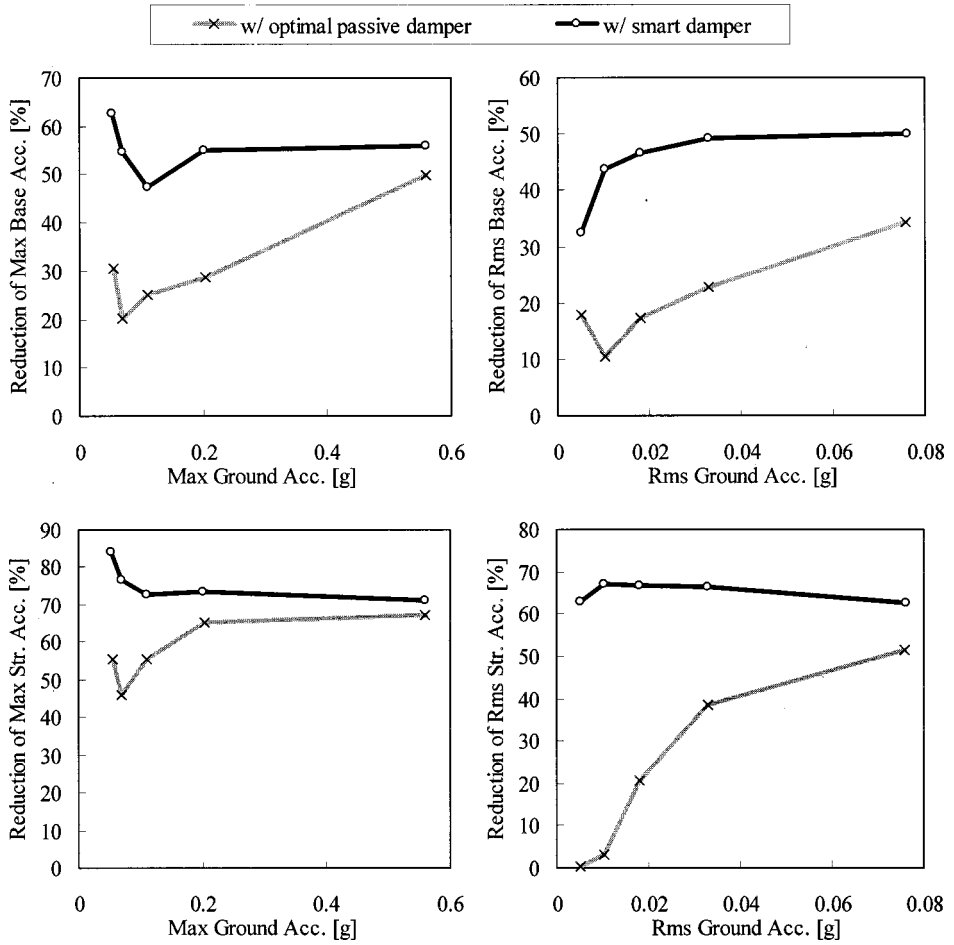

Fig. 16. Experimental results for attenuation of input ground acceleration due to scaled El Centro NS earthquake record

current being sent to the MR damper). In the passive mode, the MR damper behaves as a yielding device and approximates the behavior of lead rubber bearings. An optimization was performed experimentally to obtain the optimal passive damper configuration. As compared to this optimal hysteretic passive system, the smart isolation system achieved significant acceleration reductions over the entire range of earthquake intensities considered. These results indicate that the smart damping isolation system can be effective over a wide range of ground motion intensities and characteristics.

Acknowledgments

The writers gratefully acknowledge the partial support of this research by the National Science Foundation under Grant No. CMS 99-00234 (Dr. S. C. Liu, Program Director), by the LORD Corporation, by the Takenaka Corporation, and by a fellowship from Consejo Nacional de Investigaciones Cientificas y Técnicas (República Argentina).

References

Coleman, T., Branch, M. A., and Grace, A. (1999). *Optimization toolbox user's guide*, The MathWorks, Inc.,

Dyke, S. J., Spencer, B. F., Jr., Sain, M. K., and Carlson, J. D. (1996). ''Modeling and control of magnetorheological dampers for seismic response reduction.'' *Smart Mater. Struct.*, 5, 565–575.

Dyke, S. J., and Spencer, B. F., Jr., (1997). ''A comparison of semi-active control strategies for the MR damper.'' *Proc., IASTED Int. Conf.*, Intelligent Information Systems, The Bahamas.

Feng, M. Q., Shinozuka, M., and Fujii, S., (1993). ''Friction-controllable sliding isolated system.'' *J. Eng. Mech.*, 119(9), 1845–1864.

Furuhashi, T., et al. (1998). ''Study on micro-vibration of base isolated semiconductor factory close to Shinkansen.'' *Proc., Meetings of the Architectural Institute of Japan*, 711–718 (in Japanese).

Gavin, H. P. (2001). ''Control of seismically-excited vibration using electrorheological materials and Lyapunov methods.'' *IEEE Trans. Autom. Control*, 9(1), 27–36.

Gavin, H. P., Hanson, R. D., and Filisko, F. E. (1996). ''Electrorheological dampers part I: Analysis and design.'' *J. Appl. Mech.*, 63, 669–675.

Hall, J. F., Heaton, T. H., Halling, M. W., and Wald, D. J. (1995). ''Near-source ground motion and its effects on flexible buildings.'' *Earthquake Spectra*, 11(4), 569–605.

Heaton, T. H., Hall, J. F., Wald, D. J., and Halling, M. W. (1995). ''Response of high-rise and base-isolated buildings in a hypothetical Mw 7.0 blind thrust earthquake.'' *Science*, 267, 206–211.

Inaudi, J. A., and Kelly, J. M. (1990). ''Active isolation.'' *U.S. National Workshop on Structural Control Research*, Los Angeles, 125–130.

Inaudi, J. A., and Kelly, J. M. (1993). ''Hybrid isolation systems for equipment protection.'' *Earthquake Eng. Struct. Dyn.*, 22, 297–313.

International Conference of Building Officials. (1997). ''Uniform building code.'' *Earthquake regulations for seismic-isolated structures*, 2, Appendix, Chap. 16, Whittier, Calif.

Johnson, E. A., Ramallo, J. C., Spencer, B. F., Jr., and Sain, M. K. (1999). ''Intelligent base isolation systems.'' *Proc., 2nd World Conf. on Structural Control*, Kyoto, Japan, 367–376.

Kelly, J. M., Leitmann, G., and Soldatos, A. G. (1987). ''Robust control of base-isolated structures under earthquake excitation.'' *J. Opt.*, 53(2), 159–181.

Madden, G. J., Symans, M. D., and Wongprasert, N. (2000). ''Adaptive seismic isolation systems for structures subjected to disparate earthquake ground motions.'' *14th Analysis & Computational Specialty Conf. Proc., 2000 Structures Congress & Exposition*, Philadelphia.

Makris, N. (1997). ''Rigidity-plasticity-viscosity: Can electrorheological dampers protect base-isolated structures from near-source ground motions?'' *Earthquake Eng. Struct. Dyn.*, 26, 571–591.

Naeim, F., and Kelly, J. M. (1999). *Design of seismic isolated structures: From theory to practice*, Wiley, Chichester, England.

Nagarajaiah, S., Riley, M. A., and Reinhorn, A. (1993). ''Control of sliding-isolated bridge with absolute acceleration feedback.'' *J. Eng. Mech.*, 119(11), 2317–2332.

Nagarajaiah, S., Sahasrabudhe, S., and Iyer, R. (2000). ''Seismic response of sliding isolated bridges with smart dampers subjected to near source ground motions.'' *14th Analysis & Computational Specialty Conf. Proc., 2000 Structures Congress & Exposition*, Philadelphia.

Nishimura, H., and Kojima, A. (1998). ''Robust vibration isolation control for a seismically excited building.'' *Proc., 2nd World Conf. on Structural Control*, Kyoto, Japan, 2, 1399–1406.

Quast, P., Sain, M. K., Spencer, B. F., Jr., and Dyke, S. J. (1995). ''Microcomputer implementations of digital control strategies for structural response reduction.'' *Microcomputers in civil engineering: special issue on new directions in computer aided structural system analysis, Design Opt.*, 10, 13–25.

Ramallo, J. C., Johnson, E. A., Spencer, B. F., Jr., and Sain, M. K. (2000a). '' 'Smart' base isolation systems.'' *Proc., Advanced Technology in Structural Engineering*, Structures Congress, Philadelphia.

Ramallo, J. C., Johnson, E. A., and Spencer, B. F., Jr. (2000b). '' 'Smart' base isolation systems.'' *14th Analysis and Computational Specialty Conf. Proc., 2000 Structures Congress & Exposition*, Philadelphia.

Sahasrabudhe, S., Nagarajaiah, S., and Hard, C. (2000). ''Experimental study of sliding isolated buildings with smart dampers subjected to near source ground motions.'' *Proc., 14th Engineering Mechanics Conf.*, Austin, Tex.

Skinner, R. I., Robinson, W. H., and McVerry, G. H. (1993). *An introduction to seismic isolation*, Wiley, Chichester, England.

Spencer, B. F., Jr., Dyke, S. J., Sain, M. K., and Carlson, J. D. (1997). ''Phenomenological model of a magnetorheological damper.'' *J. Eng. Mech.*, 123(3), 230–238.

Spencer, B. F., Jr., Johnson, E. A., and Ramallo, J. C. (2000). '' 'Smart' isolation for seismic control.'' *JSME Int. J. Ser. C: Special Issue on Frontiers of Motion and Vibration Control*, 43(3), 704–711.

Symans, M. D., and Kelly, S. W. (1999). ''Fuzzy logic control of bridge structures using intelligent semi-active seismic isolation systems.'' *Earthquake Eng. Struct. Dyn.*, 28(1), 37–60.

Szucs, E. (1980). *Fundamental studies in engineering Vol. 2: Similitude and modeling*, Elsevier Scientific, Amsterdam.

Yang, J. N., et al. (1995). ''Hybrid control of seismically excited bridge structures.'' *Earthquake Eng. Struct. Dyn.*, 24(11), 1437–1451.

Yang, J. N., et al. (1996). ''Control of sliding-isolated buildings using sliding-mode control.'' *J. Struct. Eng.*, 122(2), 179–186.

Yang, J. N., and Agrawal, A. K. (2001). ''Semi-active hybrid control systems for nonlinear buildings against near-field earthquakes.'' *Eng. Struct.*, in press.

Yoshida, K., Yoshida, S., and Takeda, Y. (1999). ''Semi-active control of base isolation using feedforward information of disturbance.'' *Proc., 2nd World Conf. on Structural Control*, Kyoto, Japan, 1, 377–386.